

# Occluded Prohibited Items Detection: An X-ray Security Inspection Benchmark and De-occlusion Attention Module

Yanlu Wei\*  
weiyuanlu@buaa.edu.cn  
State Key Lab of Software  
Development Environment,  
Beihang University

Renshuai Tao\*  
rstao@buaa.edu.cn  
State Key Lab of Software  
Development Environment,  
Beihang University

Zhangjie Wu  
zhangjiewu@buaa.edu.cn  
State Key Lab of Software  
Development Environment,  
Beihang University

Yuqing Ma  
mayuqing@buaa.edu.cn  
State Key Lab of Software  
Development Environment,  
Beihang University

Libo Zhang  
libo@iscas.ac.cn  
Institute of Software Chinese  
Academy of Sciences

Xianglong Liu<sup>†</sup>  
xlliu@buaa.edu.cn  
State Key Lab of Software  
Development Environment,  
Beihang University

## ABSTRACT

Object detection has taken advantage with the advances in deep convolutional networks to bring about significant progress in recent years. Though promising results have been achieved on a multitude of situations, like pedestrian detection, autonomous driving, etc., the detection of prohibited items in X-ray images for security inspection in traffic stations like airports has received less attention. Meanwhile, security inspection often deals with a piece of baggage or suitcase where objects are randomly stacked and heavily overlapped with each other, resulting in unsatisfactory performance in detecting prohibited items in X-ray images due to the variety in scale, viewpoint, and style in these images. In this work, first, we propose an attention mechanism named De-occlusion attention module (DOAM), to deal with the problem of detecting prohibited items with some parts occluded in X-ray images. DOAM hybrids two attention sub-modules, Edge Attention Module (EAM) and the Region Attention Module (RAM), focusing on different information respectively. For the prohibited item we desire to detect, EAM emphasizes on edge information of the whole which includes both the occluded part of the item and the visible part, while RAM emphasizes region information like the texture of every point in the visible part. Second, we present a well-directed dataset targeting the problem, of which the images in the dataset are annotated manually by the professional inspectors from Beijing Capital International Airport. Our dataset, named Occluded Prohibited Items X-ray (OPIXray), which focuses on the detection of occluded prohibited items in X-ray images, consists of 8885 X-ray images of 5 categories of cutters (Fig. 1), considering the fact that cutters are the most

common prohibited items. We evaluate our method on the OPIXray dataset and compare it to several baselines, including popular methods for detection and attention mechanisms. As compared to these baselines, our method enjoys a better ability to detect the objects we desire. We also verify the ability of our method to deal with the occlusion by dividing the testing set into three subsets according to different occlusion levels and the result shows that our method achieves a better performance with a higher level of occlusion. The data and code link is <https://github.com/OPIXray-author/OPIXray>.

## CCS CONCEPTS

• **Computing methodologies** → **Object detection; Computer vision.**

## KEYWORDS

object detection, security inspection, X-ray images, occlusion.

## ACM Reference Format:

Yanlu Wei, Renshuai Tao, Zhangjie Wu, Yuqing Ma, Libo Zhang, and Xianglong Liu. 2020. Occluded Prohibited Items Detection: An X-ray Security Inspection Benchmark and De-occlusion Attention Module. In *Proceedings of the 28th ACM International Conference on Multimedia (MM '20)*, October 12–16, 2020, Seattle, United States. ACM, New York, NY, USA, 10 pages. <https://doi.org/10.1145/nnnnnnn.nnnnnnn>

## 1 INTRODUCTION

With the increasing crowd density in public transportation hubs, security inspection has become more and more important in protecting public space from safety threatening, such as terrorism. Security inspection usually adopts X-ray scanners to find whether there is any prohibited item in luggage, such as bags or suitcases. However, in this scenario, objects are randomly stacked and heavily overlapped with each other, leading to object occlusion challenge. As a result, after a long time localizing prohibited items in large amount of complex X-ray images without distraction, security inspectors struggle to accurately detect all the prohibited items, which may cause severe danger to the public. And changing shifts frequently will cost a large number of human resources, which is not advisable.

Therefore, a rapid, accurate and automatic approach to assist inspectors to detect prohibited items in X-ray scanned images is

\*Both authors contributed equally to this research.

<sup>†</sup>Corresponding author.

Permission to make digital or hard copies of all or part of this work for personal or classroom use is granted without fee provided that copies are not made or distributed for profit or commercial advantage and that copies bear this notice and the full citation on the first page. Copyrights for components of this work owned by others than ACM must be honored. Abstracting with credit is permitted. To copy otherwise, or republish, to post on servers or to redistribute to lists, requires prior specific permission and/or a fee. Request permissions from [permissions@acm.org](https://permissions.acm.org).

MM '20, October 12–16, 2020, Seattle, United States

© 2020 Association for Computing Machinery.

ACM ISBN 978-x-xxxx-xxxx-x/YY/MM... \$15.00

<https://doi.org/10.1145/nnnnnnn.nnnnnnn>

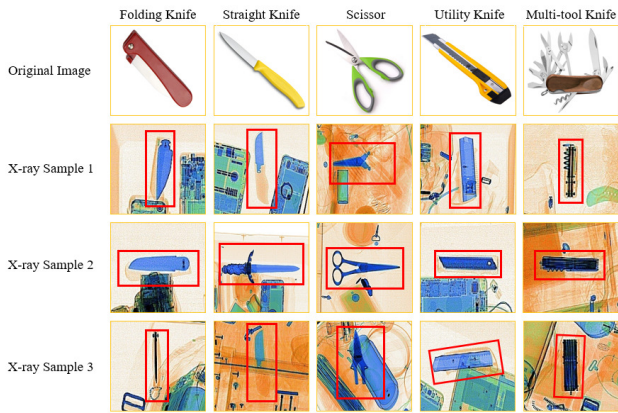


**Figure 1: Samples of the five categories of cutters and corresponding X-ray images.**

desired eagerly. As the technology of deep learning [14] especially the convolutional neural network develops [3, 35], the recognition of occluded prohibited items from X-ray pictures can be regarded as an object detection problem of computer vision, which is widely studied in the literature.

There are several works trying to solve occlusion problems in different scenarios, such as person re-identification [37, 42, 43], face recognition [6, 28, 38]. The object occlusion in Person Re-identification or Face Recognition belongs to intra-class occlusion, and every occluded object has a corresponding annotation. Therefore, a loss function can be designed by annotation information to decrease the impact of occlusion. However, object occlusion in X-ray images for security inspection often exists between prohibited items and safety items, which belongs to inter-class occlusion. In this work, what we obtained are the annotations of prohibited items, so methods of these senses can not be used for comparison.

Recently, there are also two released X-ray benchmark, namely GDXray [17] and SIXray [18]. However, GDXray [17] contains images which are grayscale, while another dataset SIXray [18] only contains less than 1% images having annotated prohibited items. And both GDXray [17] and SIXray [18] are used for classification task. As a result, both of the two datasets are inconsistent with our task that detecting occluded prohibited items.

To address above problems, we build up a dataset named Occluded Prohibited Items X-ray (OPIXray) and propose a de-occlusion attention module to handle the task of detecting occluded prohibited items in X-ray images. OPIXray contains 8885 labeled X-ray images, each of which has one or more prohibited items we desire to detect. We choose five categories of cutters as the prohibited items to detect, considering that cutter is the most common tool passengers carry. Our dataset is much more challenging in two-fold: First, items in the dataset are partitioned into five categories, where we find items belonging in different categories having similar shapes, e.g. folding knives and multi-functional knives, bringing a lot of difficulties for machines to distinguish items. Second, the item we desire to detect often escapes successfully from the sight due to the various size,

viewpoint, etc., because it can be occluded or overlapped with various items. It mimics a similar testing environment to the real-world scenario, where there are always complex viewpoints or random occlusions of item parts.

Occluded part of an item in X-ray images still provides the edge information, different from that the total information of occluded part is completely lost in natural images, inspiring us to design the edge attention module. Specifically, when viewing the cutter in an X-ray image, the edge information of the occluded part is aligned with the edge information with the visible part of the cutter. Therefore, a well-designed model can pay more attention to edge information for detection performance. Meanwhile, human inspectors recognize the cutters mainly by the help of the texture, color, etc. of the part not occluded, which we call them the region information.

With the above consideration, in this work, we develop a hybrid attention mechanism named De-occlusion Attention Module (DOAM), consisting of two major attention sub-module, Edge Attention Module (EAM) and Region Attention Module (RAM) to generate an attention distribution map as a high-quality mask for each instance. In EAM, we emphasize the effect of the edge feature during the process of modeling, by using the *sobel* operator to extract the edge image from the input X-ray image and using the edge image to produce the feature map  $F_E$  focusing on the edge information.  $F_E$  retains complete edge information of the prohibited item in the input image, which likes that security inspectors see the outline of the object. In RAM, leading the model to learn the region information of visible part of the object of interest is like that security inspectors see identifiable properties like texture, color, etc., of the object. We try to construct the relations between each position of the visible part and its neighbors, by utilizing the average pooling to aggregate the region information. This leads every position of the input image to perceive the region adjacent to it. Meanwhile, we exploit a gated convolutional network into RAM, to choose the proper size of the region for the point to perceive and generate the feature map  $F_R$  focusing on region information.

The major contributions of this work are in two-fold as follows:

- We provide a benchmark for future research in this challenging task that detecting occluded prohibited items in X-ray images for security inspection.
- We present a hybrid attention module named DOAM, which effectively integrates edge and region information we defined above, achieving satisfactory performance that outperforms popular detection approaches and attention mechanisms.

## 2 RELATED WORK

### 2.1 X-ray Images and Benchmarks

The imaging principle of the X-ray images irradiates the objects with X-ray and renders them with pseudo colors according to their spectral absorption rates. As a result, objects made of different materials in X-ray images are assigned with quite different colors, e.g., metals are often shown in blue while impenetrable objects are often shown in red. X-ray offers powerful ability in many tasks such as medical imaging analysis [1, 9, 16] and security inspection [11, 18]. Besides, the object overlapping causes X-ray images differ from natural images highly, because X-ray is often applied in the

scenarios that some objects may heavily occlude by others, *e.g.*, personal items are often randomly stacked in a piece of baggage.

Several studies in the literature have attempted to address this challenging problem and designed much work. Unfortunately, due to the particularity of security inspection, very few X-ray datasets have been published for research, and these technologies are severely affected by the occlusion caused by object overlapping. A recently released benchmark, GDXray[17] contains 19407 images, which belongs to three categories of prohibited items including gun, shuriken and razor blade. However, GDXray only contains gray-scale images in a very simple background, as well as clutters and overlaps. As a result, it is easy to recognize or detect the items in the images. SIXray[18] is a large-scale X-ray dataset which is about 100 times larger than the GDXray dataset[17]. SIXray consists of 1059231 X-ray images, but the positive samples are less than 1% to mimic a similar testing environment to the real-world scenario where inspectors often aim at recognizing prohibited items appearing in a very low frequency. Different from ours, SIXray is a dataset for the task of classification, focusing on the problem of data imbalance.

## 2.2 Attention Mechanism

Attention can be interpreted as a means of biasing the allocation of available computational resources towards the most informative components of a signal, which has been widely studied in many tasks, like image retrieval [30, 40], visual question answering [20, 41]. It captures long-range contextual information and has been widely applied in various tasks such as machine translation [34], image captioning [2], scene segmentation [5] and object recognition [32]. The work [36] is related to self-attention module, mainly exploring the effectiveness of non-local operation in space-time dimensions for videos and images. Jun Fu *et al.* [5] proposed a dual attention network (DANet) for scene segmentation by capturing contextual dependence based on the self-attention mechanism, modeling the semantic inter dependencies in spatial and channel dimensions respectively. Squeeze-and-Excitation Networks (SENet) [10] terms the Squeeze-and-Excitation block (SE), that adaptively recalibrates channel-wise feature responses by explicitly modelling inter dependencies between channels.

Different from previous works, we extend the self-attention mechanism in the task of detecting prohibited items with occlusion in X-ray images, and carefully design two types of attention modules to capture rich contextual relationships for better feature representations. Comprehensive empirical results verify the effectiveness of our proposed method.

## 2.3 Object Detection

Object detection is a classical problem in computer vision. With the rise of deep learning, CNN-based methods have become the dominant object detection solution. Most of the methods can be further divided into two general approaches: proposal-free detectors and proposal-based detectors. The first line of work follows a one-stage training strategy and does not explicitly generate proposal boxes, which is pioneered by SSD [15] and YOLO [21–23]. On the other hand, the second line, pioneered by RCNN serials [7, 8, 24], extracts class-agnostic region proposals of the potential objects from

a given image. These boxes are then further refined and classified into different categories by a specific module [24, 26, 29, 31]. An advantage of this strategy is that it can filter out many negative locations by the RPN module which facilitates the next detector task. More recently, [4, 12, 13, 33, 39] solved the problem of traditional methods relying heavily on the anchor box, with the only post-processing non-maximum suppression [19]. In this work, we make performance comparisons for our method DOAM with selected approaches from the works above as baselines to show the effectiveness of our approach.

**Table 1: The category distribution of the OPIXray dataset. Note that some images contain more than one prohibited item, the sum of all items in the different categories is greater than the total number of images.**

OPIXray	Categories					Total
	Folding	Straight	Scissor	Utility	Multi-tool	
Training	1589	809	1494	1635	1612	7109
Testing	404	235	369	343	430	1776
Total	1993	1044	1863	1978	2042	8885

## 3 THE OPIXRAY DATASET

### 3.1 Data Acquisition

In this section, we describe the construction of OPIXray dataset. These images were generated by the software, which is specially used train for professional security inspectors. The data annotation work is done by the professional security inspectors we hired from Beijing Capital International Airport. Each original X-ray image (which contains the specified prohibited items) scanned by the security inspection machine is synthesized. The synthesis still retains the property that different colors are assigned to the objects made of different materials in the X-ray images, and we localize the box-level annotations in the images with a bounding box.

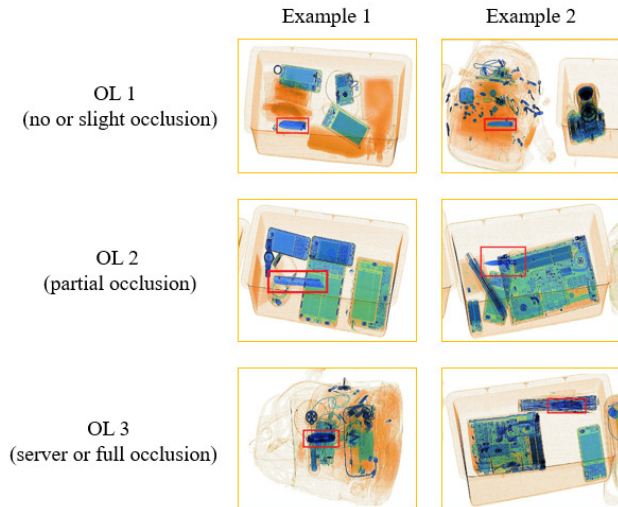
### 3.2 Dataset Properties

OPIXray dataset contains a total of 8885 X-ray images. To evaluate the ability of different models to detect different categories of prohibited items, the dataset is partitioned into a training set and a testing set, with the former containing 80% of the images (7109) and the latter containing 20% (1776), where the ratio is about 4 : 1. The dataset is further partitioned into the five common categories of prohibited items, namely, Folding Knife, Straight Knife, Scissor, Utility Knife, Multi-tool Knife. The category distribution and statistics are shown in Tab. 1.

Further, in order to study the impact brought by object occlusion levels, we divide the testing set into three subsets and name them as OL1 (occlusion level 1), OL2 (occlusion level 2) and OL3 (occlusion level 3), where the number indicates the level of item occlusion in the image (the level represents the extent to which a part of the item is occluded in the image, with 1 showing no or slight occlusion, 2 showing a partial occlusion, and 3 showing a severe or full occlusion) in Fig. 2. In OL1 and OL2, there is no or slight occlusion and partial occlusion on the objects we desire to detect in the images. To maximally explore the ability of our algorithm to deal with object

**Table 2: The category distribution of the testing set under different occlusion level settings.**

Testing set	Categories					Total
	Folding	Straight	Scissor	Utility	Multi-tool	
OL1	206	88	160	214	255	922
OL2	148	84	126	88	105	548
OL3	50	63	83	41	70	306
Total	404	235	369	343	430	1776

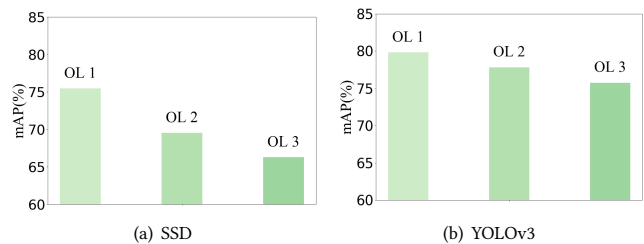
**Figure 2: Three subsets with different degrees of occlusion.**

occlusion, we construct OL3 by choosing the images with severe or full occlusion. The category distribution of the testing set under different occlusion level settings is illustrated in Tab. 2. Note that the category distribution is inconsistent obviously because our dataset mimics the real-world scenario that folding knife and multi-tool knife are more common than straight knife for passengers to bring. And the data of OL3 is significantly less than OL1 because cutters are seldom fully occluded in the real scenario. We train our model on the training set (Tab. 1), and evaluate DOAM on the each of testing subsets for the task of object occlusion. We desire that an effective model that focuses on the object occlusion problem can achieve higher performance with the increase in occlusion level on the released dataset.

### 3.3 Dataset Analysis

The OPIXray dataset brings several challenging and meaningful works to visual detection. **First**, the dataset mostly mimics a similar environment to the real-world scenario, i.e. items within personal luggage are usually stacked randomly, as shown in X-ray images in security points. Prohibited items can appear in various viewpoints, scales, etc., all of which lead to the difficulties of visual tasks. **Second**, when luggage is passed under X-ray scans, X-ray has the ability to penetrate objects, providing a measure of information on occluded parts of prohibited items. This leads to the most significant

property, object occlusion in X-ray images, which we attempt to discuss in this work in detail. As shown in Fig. 3, the performance of two famous detection methods SSD [15] and YOLOv3 [23] decreases in occlusion level of prohibited items. The performance of SSD and YOLOv3 only achieve 66.30% and 75.72% (mean Average Precision) respectively. Observing the performance of the models for the OL3 testing set, which contains items with severe occlusion, we find that our dataset really brings about challenges during object detection with occlusions. **Third**, the dataset can evaluate the ability of an approach which aims at solving object occlusion problem by comparing the improvement amount than other methods in different occlusion level settings. The improvement amount of an approach increases with the occlusion level increases, which illustrates the effectiveness of the approach to the object occlusion problems.

**Figure 3: The performance of SSD and YOLOv3 under three different object occlusion levels.**

## 4 DE-OCCLUSION ATTENTION MODULE

In this section, we first present the general framework of DOAM, which consists of two attention sub-modules, EAM and RAM, capturing edge information and the region information respectively. Further, the process of fusing the feature maps of the two sub-modules is described. Finally, we discuss the parameters of network blocks in the two attention sub-modules.

### 4.1 The General Framework of DOAM

As illustrated in Fig. 4, given an x-ray image, simulating the real-world scenario, in which objects in the luggage are placed randomly, including prohibited items we desire to detect. We employ a pre-trained network with the dilated strategy as the backbone. The input image is fed into two parallel attention modules to generate the hybrid attention map based on edge and region information of prohibited items.

We propose Edge Attention Module (EAM) to pay attention to edge information for the module during the detection process, utilizing the self-attention mechanism. To lead EAM to focus on the edge of object interested, rather than all objects in the image, we operate the edge image extracted by the edge detection operation from the input image, and optimize the particular loss function so as to generate the feature map  $F_E$  which emphasizes edge information of prohibited items.  $F_E$  retains complete edge information of the prohibited item in the input image, which likes that security inspectors see the outline of the object.

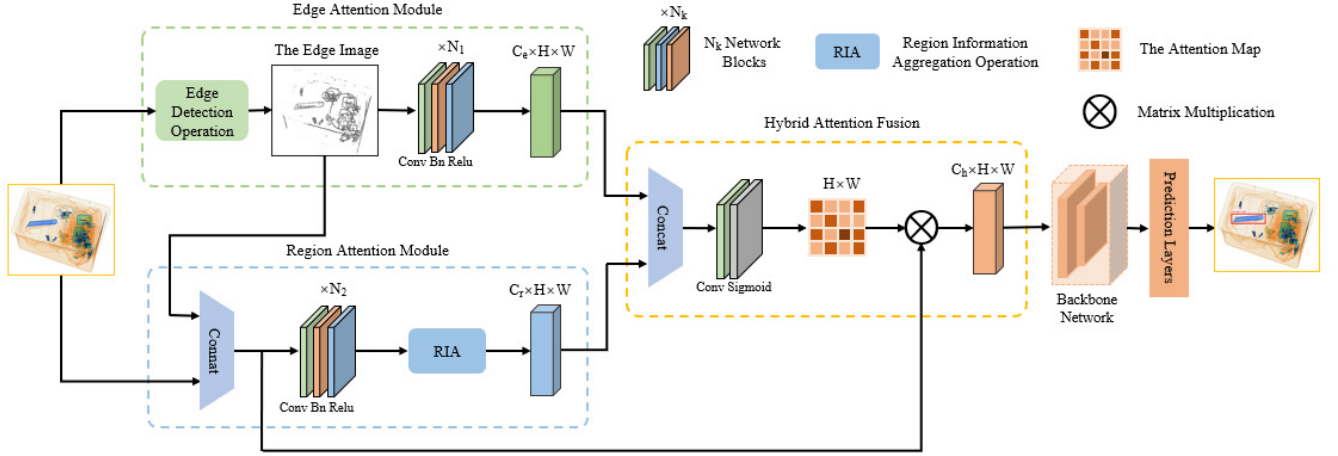


**Figure 4: DOAM integrated with a general backbone network architecture. As illustrated, DOAM hybrids two attention sub-modules, Edge Attention Module (EAM) and Region Attention Module (RAM), focusing on different information respectively. Further, it fuses the two feature maps to generate an attention map and apply the attention map to the input image to generate the refined feature map we desire. Finally the refined feature map can be utilized by any architectures integrated.**

To imitate that security inspectors recognize prohibited items by identifying properties like texture, color, etc., of visible part, we propose Region Attention Module (RAM) to enhance the ability of learning region information of visible part. The aggregation of regional information enables each point of the feature map to perceive the information of a certain region (the region size can be defined by ourselves) around it, enhancing the relation between the point and the certain region around it. Like EAM, the feature map  $F_R$  which emphasizes region information of prohibited items is generated, remaining information of identifiable properties of the visible part of prohibited items.

We fuse the two feature maps  $F_E$  and  $F_R$  to generate an attention map by a series of operations, and finally apply the attention map to the original data to generate the feature map we desire. The entire process of the attention mechanism is detailed in Algorithm 1.

## 4.2 Edge Attention Module (EAM)

Next, we elaborate the process used by EAM to adaptively focus on the whole edge information of the prohibited item. Suppose there are  $n$  training images in the dataset  $X = \{x_1, \dots, x_n\}$ . For each input image  $x \in X$ , we utilize the convolutional neural network with the horizontal and vertical kernel denoted as  $s_h, s_v$  of the *Sobel* operator, to respectively compute the edge images  $PE^h$  and  $PE^v$  for the horizontal and vertical directions. We further generate the edge picture  $PE$  of the input image  $x$  by synthesizing the above two results  $PE^h$  and  $PE^v$ . However, this operation detects edges of all items in the image, both prohibited and safety. Therefore, concatenating  $PE$  and the input RGB image  $x$ , as a feature fusion operation, strengthens the edge information of all objects in the image. To lead EAM to magnify edge information of object interested only, we use  $N_1$  network blocks (Here, we define  $N_1$  as the attention intensity of EAM, which represents that the performance of the attention module changes with the value of  $N_1$ . And the

### Algorithm 1 The Operation Process of DOAM.

- 1: **Input:** an X-ray image  $x \in \mathbb{R}^{C \times H \times W}$ ;
- 2: calculate the horizontal edge image  $PE^h$ .
- 3: calculate the vertical edge image  $PE^v$ .
- 4: generate the edge image  $PE$ .
- 5: **for**  $N_1$  steps **do**
- 6:     update the feature map  $F_E$  by the network block.
- 7: **end for**
- 8: concatenate  $x$  and  $PE$ .
- 9: **for**  $N_2$  steps **do**
- 10:     update the feature map  $A$  by the network block.
- 11: **end for**
- 12: **for**  $k \in \{k_1, \dots, k_n\}$  **do**
- 13:     update the feature map set  $S = \{B^{k_1}, \dots, B^{k_n}\}$
- 14: **end for**
- 15: concatenate  $A$  with each  $B^k$  in  $S$ .
- 16: generate the feature map  $F_R$  by the gated conv net.
- 17: concatenate  $F_E$  and  $F_R$ .
- 18: generate the feature map  $F_{mix}$ .
- 19: calculate the attention map  $S = \sigma(F_{mix})$ .
- 20: generate the feature map  $M$ .
- 21: **Output:** the feature map  $M \in \mathbb{R}^{C_h \times H \times W}$ .

proper value of  $N_1$  will be discussed later), in which each block consists of a convolutional layer with a  $3 \times 3$  kernel size, a batch normalization layer, and a relu layer, to extract the feature map  $F_E$  of the edge image  $PE$ . The operations can be formulated as follows:

$$F_E = \{relu(W_e \cdot PE + b_e)\}_{N_1}. \quad (1)$$

where  $\{\cdot\}_{N_1}$  means that the operation is repeated  $N_1$  times,  $W_e, b_e$  are parameters of the convolutional layer. After extracting the feature map  $F_E$  as shown in Eq. 1 above, we adaptively attend to

the edge information of the prohibited item within the feature map  $F_E$  by optimizing a specific loss function.

### 4.3 Region Attention Module (RAM)

For every point of the feature map, in order to construct relations between each position and a certain region around it, we utilize  $N_2$  network blocks (As we state in EAM,  $N_2$  is the attention intensity of RAM and the value of  $N_2$  will be discussed later), in which each block consists a convolutional layer with the kernel size is  $3 \times 3$ , a batch normalization layer, a relu layer, to extract the feature map  $A$  from the concatenated image (concatenating the input image  $x$  with its corresponding edge image  $PE$ ) as follows:

$$A = \{relu(W_r \cdot (x || PE) + b_r)\}_{N_2}. \quad (2)$$

where  $||$  represents concatenating operation. We further generate the resulting feature map  $FR$  of the RAM by refining  $A$  through the region information aggregation (RIA) operation.

Fig. 5 illustrates the structure of RIA operation. For the input feature map  $A$ , RIA operation aggregates the information of different scales of regions around it by utilizing the different scales of kernels and average pool operators. For the convenience of successive concatenation, we further expand the feature maps after the average pool layer to the size of the original feature map  $A$ , generating the corresponding feature map set  $\{B^{k_1}, \dots, B^{k_n}\}$ . These operations can be formulated as follows:

$$B_{ij}^k = \frac{\sum_{m=i-(i \bmod k)+k}^{i-(i \bmod k)+k} \sum_{n=j-(j \bmod k)+k}^{j-(j \bmod k)+k} A_{mn}}{k^2}. \quad (3)$$

where  $B_{ij}^k$  represents the feature of the  $i$ -th row and  $j$ -th column of feature map  $B$ , when the scale of the kernel for the average pool operator is  $k$ .

We further concatenate the two feature maps ( $B$  and  $A$ ) in the dimension of channel to generate a new feature map, where the dimensions are  $2C_r \times H \times W$ . Then every point of the new feature map has the ability to perceive the region of size  $k * k$  around it, which means that we have successfully constructed the relations.

Note that the size of the region perceived has a great influence on detection performance, and the size varies with different scales of prohibited items. In order to enable RIA operation to perform well on various scales of prohibited items, it is necessary to design a mechanism to adaptively choose an optimal value for  $k$ . We exploit a gated convolutional neural network  $\mathbb{G}$  with  $3 \times 3$  kernels into RIA, to select the proper feature map  $F_{RAM}$  from the feature map set  $\{B^{k_1}, \dots, B^{k_n}\}$  as output. The operations are formulated as follows:

$$FR = \mathbb{G}(B^{k_1} || A, \dots, B^{k_n} || A). \quad (4)$$

where  $||$  represents concatenating operation.

### 4.4 Hybrid Attention Fusion

As is illustrated in Algorithm 1, for the result feature maps  $F_{EAM}$  and  $F_{RAM}$  outputted by the EAM and the RAM respectively, where  $F_E \in \mathbb{R}^{C_e \times H \times W}$ ,  $F_R \in \mathbb{R}^{C_r \times H \times W}$ , we concatenate them for information fusion. And further we feed the concatenated feature into a convolutional layer, where the kernel size is  $1 \times 1$ , to generate the feature map  $F_{mix} \in \mathbb{R}^{(C_e+C_r) \times H \times W}$ , which have confused the edge

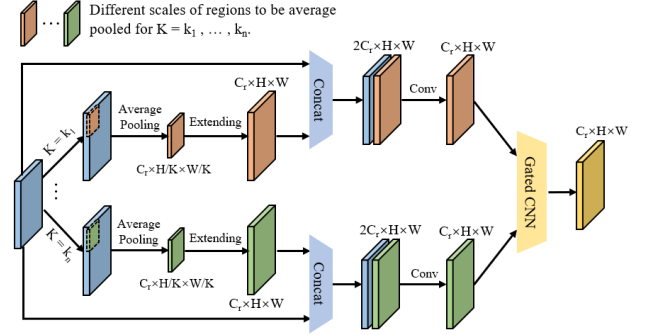


Figure 5: The Operation Process of RIA.

information and the regional information, both strengthened. The operation can be formulated as follows:

$$F_{mix} = W_m (F_E || F_R) + b_m. \quad (5)$$

where  $||$  represents the operation of concatenating, and  $W_m$ ,  $b_m$  are parameters of the convolutional layer. Then we utilize the feature map  $F_{mix}$  as the input of a sigmoid function to generate the attention map  $S$  as follows:

$$S = \sigma(F_{mix}) = \frac{1}{1 + e^{-F_{mix}}}. \quad (6)$$

where  $S \in \mathbb{R}^{H \times W}$ . Finally, we calculate the inner product of the attention map  $S$  and the concatenated image (concatenating the input image  $x$  and the edge image  $PE$ ) as follows:

$$M_j = \sum_{i=1}^{H \times W} (S_{ji} (x_i || PE_i)). \quad (7)$$

where  $M \in \mathbb{R}^{C_h \times H \times W}$ , and it is the feature map we desire where the features which highly contribute to the detection of the prohibited item are magnified.

### 4.5 Discussions of Attention Intensities

In this section, we analyse the two attention intensities,  $N_1$  of EAM and  $N_2$  of RAM, which are defined in above sections. The value of attention intensity means the number of convolutional layers. Choosing appropriate values of  $N_1$  and  $N_2$  can not only improve the performance, but also effectively reduce the complexity and improve the executive efficiency of DOAM. Therefore, we design the experiments to investigate the impacts on the performance of different values of  $N_1$  and  $N_2$ , and the performances are illustrated in Fig. 6.

As we can see from Fig. 6, the values of the network blocks  $N_1$  (Eq. 1) and  $N_2$  (Eq. 2) in EAM and RAM have an obvious impact on the performance of the model. Usually that the performance of a model increases with the number of the convolution layers, which mainly applicable to the case with enough data. However, when the data is hungry, complex network causes the overfitting easily, leading to the poor generalization ability of the model. We construct the network structure according to the experiment of parameter comparison, which highly matches the OPIXray dataset. When both the number of the network blocks  $N_1$  (Eq. 1) and  $N_2$  (Eq.

2) in EAM and RAM are 5, we get the best result that both of them are 5. And all the experiments following are designed by utilizing the network structure with the two values.

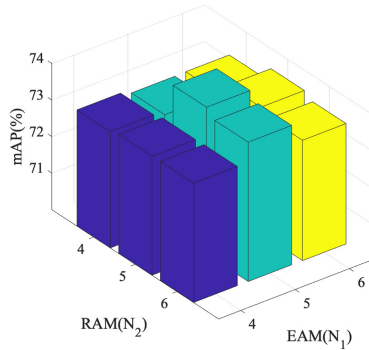


**Figure 6: Performance comparison of DOAM with different values of the attention intensities of EAM and RAM.**

**Table 3: Performance comparison between DOAM and other different attention mechanisms on object categories. FO, ST, SC, UT and MU represent Folding Knife, Straight Knife, Scissor, Utility Knife and Multi-tool Knife, respectively.**

Method	mAP	Categories				
		FO	ST	SC	UT	MU
SSD [15]	70.89	76.91	35.02	93.41	65.87	83.27
SSD+SE [10]	71.85	77.17	38.29	92.03	66.10	<b>85.67</b>
SSD+Non-local [36]	71.41	77.55	36.38	<b>95.26</b>	64.86	82.98
SSD+DA [5]	71.96	79.68	37.69	93.38	64.14	84.90
<b>SSD+DOAM(ours)</b>	<b>74.01</b>	<b>81.37</b>	<b>41.50</b>	95.12	<b>68.21</b>	83.83

## 5 EXPERIMENTS

In this section, we carry on extensive experiments to evaluate the DOAM we proposed. In order to perform better apple-to-apple comparisons, we reproduced all the evaluated networks in the PyTorch framework and report our reproduced results in the whole experiments.

We first verify that DOAM outperforms all the attention mechanisms mentioned above, over different categories and different occlusion levels. To thoroughly evaluate the effectiveness of DOAM, further we perform ablation experiments. Finally, we demonstrate the general applicability of DOAM across different architectures and the effectiveness after DOAM-integrated. One can seamlessly integrate DOAM in any CNN architectures and jointly train the combined DOAM-integrated networks. Fig. 4 shows a diagram of DOAM integrated with the base architecture SSD as an example.

In all experiments following, all models are optimized by the SGD optimizer and the learning rate is set to 0.0001. The batch size is set to 24 and the momentum and weight decay are set to 0.9 and 0.0005 respectively. We evaluate the mean Average Precision (mAP) of the object detection to measure the performance of the

model and the IOU threshold is set to 0.5. We further select the best performance model to calculate the AP of each category to observe the performance improvement on different categories. Furthermore, in order to avoid the influence of image data modification on edge image generation, we do not use any data augmentation methods to expand the data or modify the pixel value of the original image, which helps us to better analyze the impact of edge information.

### 5.1 Comparing with Different Attention Mechanisms

We experimentally verify the effectiveness of DOAM on different categories and different occlusion levels of OPIXray dataset. We compare three variants of attention mechanisms, including SENet [10], Non-local Net [36] and DANet [5], where the attention modules are called SE, Non-local and DA. The three attention mechanisms focus on channel attention, spatial attention and combining both channel and spatial attention, respectively. All experiments in this subsection are designed on the base architecture of SSD [15]. Tab. 3 and 4 show the experiment results of various module-integrated networks on different categories and different occlusion levels, respectively. As we can observe from the two tables, DOAM surpasses these current popular attention networks obviously.

**Experiments on Object Categories.** We experimentally verify the effectiveness of DOAM on different object categories, and the training and testing data of all module-integrated networks are illustrated in Tab. 1. As we can observe from Tab. 3, the performance of DOAM has improved 2.16%, 2.60%, 2.05%, compared with SENet [10], Non-local Net [36] and DANet [5], respectively. The attention mechanism DOAM is superior to general attention mechanisms on different object categories.

The performance improvement DOAM brings depends on the levels of the occlusion. Tab. 3 shows the improvement of DOAM is mainly reflected in straight knives, folding knives and utility knives, all of which are with the high level occlusion, which are we expected. Especially for the straight knives, which are the category, of knives with highest level occlusion, the performance is improved by an impressive amount of 6.48% compared with the baseline, and 3.21% compared with SENet [10] which achieves the best performance on the straight knives among three attention mechanisms. For the scissors, the lightest occlusion category, the performance is only improved by 1.71% compared with the baseline and similar to the Non-local Net [36], achieves the best performance on the scissors compared to the other four types of knives. By strengthening whole edge information and visual parts region information of prohibited item, DOAM greatly alleviates the problem of the feature information loss caused by the occlusion in X-ray images.

**Experiments on Object Occlusion Levels.** We experimentally verify the effectiveness of DOAM on different occlusion levels. We divide the testing set into three sub-sets according to occlusion levels as Tab. 2 illustrates. All module-integrated networks are trained by training set data in Tab. 1, in which the data distribution of each category is uniform, containing all three occlusion levels. And each of the trained models is tested on OL1, OL2 and OL3 respectively. The experimental results are shown in Tab. 4. We observe not only the improvement over the baseline SSD [15] and the general attention mechanisms with the best performance in

**Table 4: Performance comparison between DOAM and other different attention mechanisms on object occlusion levels.**

Method	OL 1	OL 2	OL 3
SSD [15]	75.45	69.54	66.30
SSD+SE [10]	76.02	70.11	67.53
SSD+Non-local [36]	75.99	70.17	65.87
SSD+DA [5]	77.41	69.68	66.93
<b>SSD+DOAM(ours)</b>	<b>77.87</b>	<b>72.45</b>	<b>70.78</b>

the corresponding occlusion level. We expect to see that DOAM surpasses these current popular attention networks on all occlusion levels and the improvement increases with the occlusion level increases, the effectiveness of our model to solve object occlusion is verified.

In Fig. 7, we can clearly obtain a conclusion that DOAM can achieve a higher performance than the baseline and other attention mechanisms with the X-ray images suffer a higher level of occlusion. It verifies the effectiveness of DOAM that it has a significant effect on the performance of detecting occluded prohibited items in X-ray images.

## 5.2 Ablation Studies

In this subsection, we empirically show the effectiveness of our design choice. For ablation study, we use OPIXray dataset and adopt SSD as the base architecture. The results are shown in Tab. 5.

Our module design process is split into four steps in detail. First, We concatenate the input image and the corresponding edge image. Second, we search for the effective approach to computing the edge attention. Third, we compute the region attention (without drawing any gated convolutional networks) and combine both channel and spatial attention modules. Finally, we draw a gated convolutional network into the region attention module. We explain the details of each experiment below.

We observe that the EAM improved the performance by 0.43% compared with the method of simply concatenating the input image and the corresponding edge image without any attention mechanism operations. We argue it is mainly because the EAM has the ability to pay the attention adaptively to the prohibited items we desire to detect by specifically increasing the weight of edge information through the optimization of a loss function. However, simply concatenating operates all the objects in the image equally whether the object is we desire to detect or not for feature fusion.

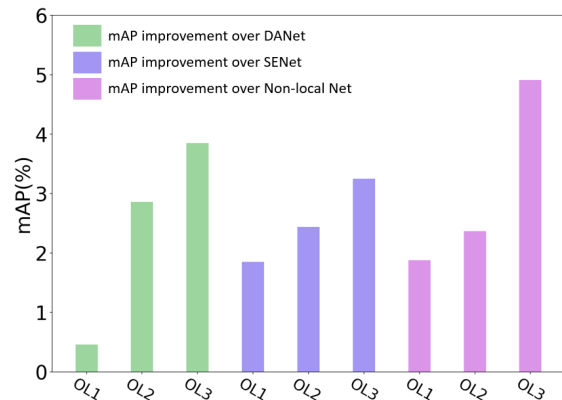
Next, we experimentally verify that using both edge attention module and region attention module enables finer attention inference than the edge attention module alone. To enhance relations of regions, we try to make every pixel of the feature map has the ability to perceive the information of a certain area around it because it is beneficial for the RAM to focus on the non-occluded parts of the objects which have greater impacts on the prediction when optimizing by the loss function. Note that we observe prohibited item size is about  $10 \times 10$  averagely, so we choose  $10 \times 10$  as the region scale to perceive for each position of the feature map. The results in Tab. 5 show that the performance of  $\tilde{\text{AJEAM}} + \text{RAM}$  is 0.37%

higher than that of EAM alone, which confirms the correctness of our assumption.

Given the region-wise refined features, we explore an effective method to select the best size of the region to perceive adaptively. We choose three different scales of the regions ( $5 \times 5$ ,  $10 \times 10$ ,  $15 \times 15$  respectively), and draw a gated convolutional neural network (GCNN) into RAM, to adaptively select the best feature map which generated by operation of average pooling with appropriate pooling size. The experimental results show that after drawing the GCNN, the performance improves by 0.9%.

**Table 5: Ablation studies of DOAM. C represents simply concatenate operation, E represents Edge Attention Module, R represents Region Attention Module, and G represents Gate Convolutional Neural Network (GCNN).**

Method	mAP	Category				
		FO	ST	SC	UT	MU
SSD [15]	70.89	76.91	35.02	93.41	65.87	83.27
SSD+C	72.32	79.00	36.46	94.13	68.85	83.18
SSD+E	72.75	80.26	35.54	94.81	67.96	<b>85.19</b>
SSD+E+R(without G)	73.12	79.94	38.58	93.39	<b>69.40</b>	84.28
<b>SSD+DOAM(E+R)</b>	<b>74.01</b>	<b>81.37</b>	<b>41.50</b>	<b>95.12</b>	68.21	83.83

**Figure 7: The amount changes of performance improvement of DOAM with occlusion level increases.**

## 5.3 Comparing with Different Detection Approaches

To further evaluate the effectiveness of DOAM and verify DOAM can be applied to various detection networks, we conduct experiments on the famous detection approaches, SSD [15], YOLOv3 [23] and FCOS [33]. The results are shown in Tab. 6.

As we can see from Tab. 6, the performance of DOAM-integrated networks are improved by 3.12% and 1.04% compared with original SSD and YOLOv3, respectively. However, the performances on the folding knives and the scissors after DOAM-integrated are slightly reduced. We speculate that the reason is that these images of the

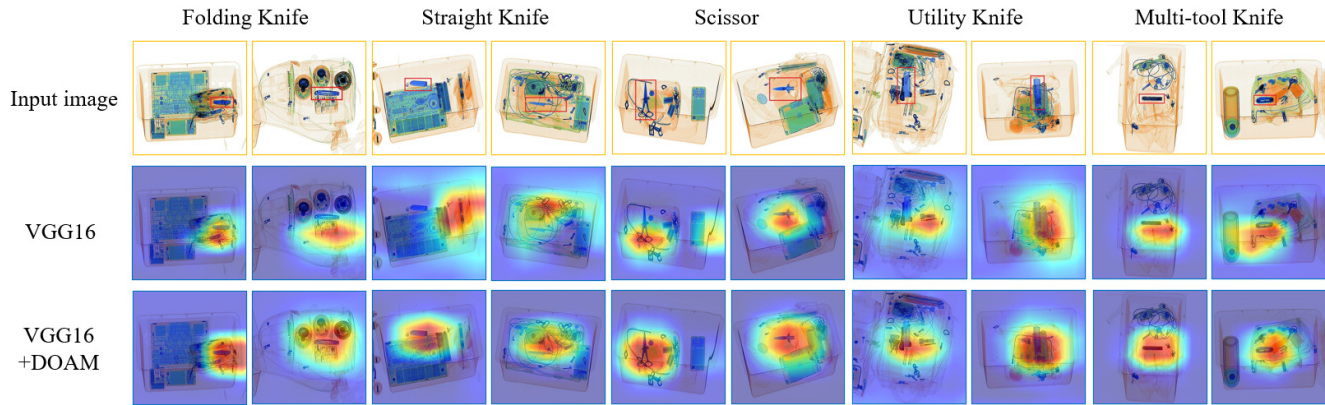


Figure 8: Grad-CAM [25] visualization results. We compare the visualization results of the DOAM-integrated network (VGG16+DOAM) with baseline (VGG16). The grad-CAM visualization is calculated for the last convolutional outputs. The ground-truth label is shown on the top of each input image.

Table 6: Performance comparison between DOAM-integrated network and baselines for three famous detection approaches.

Method	mAP	Category				
		FO	ST	SC	UT	MU
SSD [15]	70.89	76.91	35.02	93.41	65.87	83.27
<b>SSD+DOAM(ours)</b>	<b>74.01</b>	<b>81.37</b>	<b>41.50</b>	<b>95.12</b>	<b>68.21</b>	<b>83.83</b>
YOLOv3 [23]	78.21	92.53	36.02	<b>97.34</b>	70.81	94.37
<b>YOLOv3+DOAM(ours)</b>	<b>79.25</b>	<b>90.23</b>	<b>41.73</b>	96.96	<b>72.12</b>	<b>95.23</b>
FCOS [33]	82.02	86.41	68.47	90.22	78.39	86.60
<b>FCOS+DOAM(ours)</b>	<b>82.41</b>	<b>86.71</b>	<b>68.58</b>	<b>90.23</b>	<b>78.84</b>	<b>87.67</b>

two categories in the dataset are occluded not seriously. When the occlusion level increases, the attention mechanism pays more attention to the objects occluded highly like straight knives while less attention to the objects occluded slightly, which results in the slight performance degradation for folding knives and scissors.

#### 5.4 Network Visualization with Grad-CAM

For the visualization analysis, we apply the Grad-CAM [25] to the two networks, VGG16 network [27] and DOAM-integrated network (VGG16+DOAM), and using images from the OPIXray dataset. As we can clearly see from Fig. 8 that the Grad-CAM masks of DOAM cover the target object regions more widely than the single VGG16 network [27], which verifies the effectiveness of RAM, utilizing the RIA to aggregate the region information. And the Grad-CAM masks of the DOAM cover the target object more evenly, circling the shape of the target object, due to the operation by EAM, which focuses on the edge information. From the observations, we conjecture that the feature refinement process of our model eventually leads the networks to perform better.

## 6 CONCLUSION

In this paper, we investigate occluded prohibited items detection in X-ray scanned images, which is a promising application in industry yet remains fewer studied in computer vision. To facilitate research in this field, we present OPIXray dataset, a dataset mainly focusing on occlusion of the objects in the images. All the backgrounds of which were captured from the real-world scenarios and the prohibited items were inserted by the security inspectors we hired from Beijing Capital International Airport, which make the OPIXray dataset cover complicated scenarios and professional. We manually localize the box-level annotations in the images with a bounding box according to the statement provided by these professional security inspectors.

Motivated by filtering irrelevant information, we present a hybrid attention mechanism named DOAM, which can be applied to various popular detection approaches, to refine the features. In practice, we design two attention sub-modules, EAM and RAM, focusing on the information interested respectively. As shown in experiments, DOAM surpasses popular attention mechanisms and the DOAM-integrated network surpasses popular detection approaches obviously, establishing a strong baseline for the proposed task.

## REFERENCES

- [1] Arjun Chaudhary, Abhishek Hazra, and Prakash Chaudhary. 2019. Diagnosis of Chest Diseases in X-Ray images using Deep Convolutional Neural Network. In *2019 10th International Conference on Computing, Communication and Networking Technologies (ICCCNT)*. IEEE, 1–6.
- [2] Long Chen, Hanwang Zhang, Jun Xiao, Liqiang Nie, Jian Shao, Wei Liu, and Tat-Seng Chua. 2017. Sca-cnn: Spatial and channel-wise attention in convolutional networks for image captioning. In *Proceedings of the IEEE conference on computer vision and pattern recognition*. 5659–5667.
- [3] Zhi-Qi Cheng, Jun-Xiu Li, Qi Dai, Xiao Wu, Jun-Yan He, and Alexander G Hauptmann. 2019. Improving the learning of multi-column convolutional neural network for crowd counting. In *Proceedings of the 27th ACM International Conference on Multimedia*. 1897–1906.
- [4] Kaiwen Duan, Song Bai, Lingxi Xie, Honggang Qi, Qingming Huang, and Qi Tian. 2019. Centernet: Keypoint triplets for object detection. In *Proceedings of the IEEE International Conference on Computer Vision*. 6569–6578.
- [5] Jun Fu, Jing Liu, Haijie Tian, Yong Li, Yongjun Bao, Zhiwei Fang, and Hanqing Lu. 2019. Dual attention network for scene segmentation. In *Proceedings of the IEEE Conference on Computer Vision and Pattern Recognition*. 3146–3154.
- [6] Shiming Ge, Jia Li, Qiting Ye, and Zhao Luo. 2017. Detecting masked faces in the wild with lle-cnns. In *Proceedings of the IEEE Conference on Computer Vision and Pattern Recognition*. 2682–2690.
- [7] Ross Girshick. 2015. Fast r-cnn. In *Proceedings of the IEEE international conference on computer vision*. 1440–1448.
- [8] Ross Girshick, Jeff Donahue, Trevor Darrell, and Jitendra Malik. 2014. Rich feature hierarchies for accurate object detection and semantic segmentation. In *Proceedings of the IEEE conference on computer vision and pattern recognition*. 580–587.
- [9] Shuai Guo, Songyuan Tang, Jianjun Zhu, Jingfan Fan, Danni Ai, Hong Song, Ping Liang, and Jian Yang. 2019. Improved U-Net for Guidewire Tip Segmentation in X-ray Fluoroscopy Images. In *Proceedings of the 2019 3rd International Conference on Advances in Image Processing*. 55–59.
- [10] Jie Hu, Li Shen, and Gang Sun. 2018. Squeeze-and-excitation networks. In *Proceedings of the IEEE conference on computer vision and pattern recognition*. 7132–7141.
- [11] Shengling Huang, Xin Wang, Yifan Chen, Jie Xu, Tian Tang, and Baozhong Mu. 2019. Modeling and quantitative analysis of X-ray transmission and backscatter imaging aimed at security inspection. *Optics express* 27, 2 (2019), 337–349.
- [12] Hei Law and Jia Deng. 2018. Cornernet: Detecting objects as paired keypoints. In *Proceedings of the European Conference on Computer Vision (ECCV)*. 734–750.
- [13] Hei Law, Yun Teng, Olga Russakovsky, and Jia Deng. 2019. Cornernet-lite: Efficient keypoint based object detection. *arXiv preprint arXiv:1904.08900* (2019).
- [14] Yann LeCun, Yoshua Bengio, and Geoffrey Hinton. 2015. Deep learning. *nature* 521, 7553 (2015), 436–444.
- [15] Wei Liu, Dragomir Anguelov, Dumitru Erhan, Christian Szegedy, Scott Reed, Cheng-Yang Fu, and Alexander C Berg. 2016. Ssd: Single shot multibox detector. In *European conference on computer vision*. Springer, 21–37.
- [16] Jianjie Lu and Kai-yu Tong. 2019. Towards to Reasonable Decision Basis in Automatic Bone X-Ray Image Classification: A Weakly-Supervised Approach. In *Proceedings of the AAAI Conference on Artificial Intelligence*, Vol. 33. 9985–9986.
- [17] Domingo Mery, Vladimir Riffo, Uwe Zscherpel, German Mondragon, Iván Lillo, Irene Zuccar, Hans Lobel, and Miguel Carrasco. 2015. GDXray: The database of X-ray images for nondestructive testing. *Journal of Nondestructive Evaluation* 34, 4 (2015), 42.
- [18] Caijing Miao, Lingxi Xie, Fang Wan, Chi Su, Hongye Liu, Jianbin Jiao, and Qixiang Ye. 2019. Sixray: A large-scale security inspection x-ray benchmark for prohibited item discovery in overlapping images. In *Proceedings of the IEEE Conference on Computer Vision and Pattern Recognition*. 2119–2128.
- [19] Alexander Neubeck and Luc Van Gool. 2006. Efficient non-maximum suppression. In *18th International Conference on Pattern Recognition (ICPR'06)*, Vol. 3. IEEE, 850–855.
- [20] Liang Peng, Yang Yang, Zheng Wang, Xiao Wu, and Zi Huang. 2019. CRA-Net: Composed Relation Attention Network for Visual Question Answering. In *Proceedings of the 27th ACM International Conference on Multimedia*. 1202–1210.
- [21] Joseph Redmon, Santosh Divvala, Ross Girshick, and Ali Farhadi. 2016. You only look once: Unified, real-time object detection. In *Proceedings of the IEEE conference on computer vision and pattern recognition*. 779–788.
- [22] Joseph Redmon and Ali Farhadi. 2017. YOLO9000: better, faster, stronger. In *Proceedings of the IEEE conference on computer vision and pattern recognition*. 7263–7271.
- [23] Joseph Redmon and Ali Farhadi. 2018. Yolov3: An incremental improvement. *arXiv preprint arXiv:1804.02767* (2018).
- [24] Shaoqing Ren, Kaiming He, Ross Girshick, and Jian Sun. 2015. Faster r-cnn: Towards real-time object detection with region proposal networks. In *Advances in neural information processing systems*. 91–99.
- [25] Ramprasaath R Selvaraju, Michael Cogswell, Abhishek Das, Ramakrishna Vedantam, Devi Parikh, and Dhruv Batra. 2017. Grad-cam: Visual explanations from deep networks via gradient-based localization. In *Proceedings of the IEEE international conference on computer vision*. 618–626.
- [26] Abhinav Shrivastava, Rahul Sukthankar, Jitendra Malik, and Abhinav Gupta. 2016. Beyond skip connections: Top-down modulation for object detection. *arXiv preprint arXiv:1612.06851* (2016).
- [27] Karen Simonyan and Andrew Zisserman. 2014. Very deep convolutional networks for large-scale image recognition. *arXiv preprint arXiv:1409.1556* (2014).
- [28] Lingxue Song, Dihong Gong, Zhifeng Li, Changsong Liu, and Wei Liu. 2019. Occlusion Robust Face Recognition Based on Mask Learning With Pairwise Differential Siamese Network. In *Proceedings of the IEEE International Conference on Computer Vision*. 773–782.
- [29] Ke Sun, Bin Xiao, Dong Liu, and Jingdong Wang. 2019. Deep high-resolution representation learning for human pose estimation. In *Proceedings of the IEEE Conference on Computer Vision and Pattern Recognition*. 5693–5703.
- [30] Xie Sun, Lu Jin, and Zechao Li. 2019. Attention-Aware Feature Pyramid Ordinal Hashing for Image Retrieval. In *Proceedings of the ACM Multimedia Asia on ZZZ*. 1–6.
- [31] Christian Szegedy, Sergey Ioffe, Vincent Vanhoucke, and Alexander A Alemi. 2017. Inception-v4, inception-resnet and the impact of residual connections on learning. In *Thirty-first AAAI conference on artificial intelligence*.
- [32] Jinhui Tang, Lu Jin, Zechao Li, and Shenghua Gao. 2015. RGB-D object recognition via incorporating latent data structure and prior knowledge. *IEEE Transactions on Multimedia* 17, 11 (2015), 1899–1908.
- [33] Zhi Tian, Chunhua Shen, Hao Chen, and Tong He. 2019. Fcos: Fully convolutional one-stage object detection. In *Proceedings of the IEEE International Conference on Computer Vision*. 9627–9636.
- [34] Ashish Vaswani, Noam Shazeer, Niki Parmar, Jakob Uszkoreit, Llion Jones, Aidan N Gomez, Łukasz Kaiser, and Illia Polosukhin. 2017. Attention is all you need. In *Advances in neural information processing systems*. 5998–6008.
- [35] Pichao Wang, Zhaoyang Li, Yonghong Hou, and Wanqing Li. 2016. Action recognition based on joint trajectory maps using convolutional neural networks. In *Proceedings of the 24th ACM international conference on Multimedia*. 102–106.
- [36] Xiaolong Wang, Ross Girshick, Abhinav Gupta, and Kaiming He. 2018. Non-local neural networks. In *Proceedings of the IEEE conference on computer vision and pattern recognition*. 7794–7803.
- [37] Xinlong Wang, Tete Xiao, Yuning Jiang, Shuai Shao, Jian Sun, and Chunhua Shen. 2018. Repulsion loss: Detecting pedestrians in a crowd. In *Proceedings of the IEEE Conference on Computer Vision and Pattern Recognition*. 7774–7783.
- [38] Jian Yang, Lei Luo, Jianjun Qian, Ying Tai, Fanlong Zhang, and Yong Xu. 2016. Nuclear norm based matrix regression with applications to face recognition with occlusion and illumination changes. *IEEE transactions on pattern analysis and machine intelligence* 39, 1 (2016), 156–171.
- [39] Ze Yang, Shaohui Liu, Han Hu, Liwei Wang, and Stephen Lin. 2019. Reppoints: Point set representation for object detection. In *Proceedings of the IEEE International Conference on Computer Vision*. 9657–9666.
- [40] Xingxu Yao, Dongyu She, Sicheng Zhao, Jie Liang, Yu-Kun Lai, and Jufeng Yang. 2019. Attention-aware polarity sensitive embedding for affective image retrieval. In *Proceedings of the IEEE International Conference on Computer Vision*. 1140–1150.
- [41] Zheng-Jun Zha, Jiawei Liu, Tianhao Yang, and Yongdong Zhang. 2019. Spatiotemporal-Textual Co-Attention Network for Video Question Answering. *ACM Transactions on Multimedia Computing, Communications, and Applications (TOMM)* 15, 2s (2019), 1–18.
- [42] Shifeng Zhang, Longyin Wen, Xiao Bian, Zhen Lei, and Stan Z Li. 2018. Occlusion-aware R-CNN: detecting pedestrians in a crowd. In *Proceedings of the European Conference on Computer Vision (ECCV)*. 637–653.
- [43] Chunlun Zhou and Junsong Yuan. 2018. Bi-box regression for pedestrian detection and occlusion estimation. In *Proceedings of the European Conference on Computer Vision (ECCV)*. 135–151.